Fermi National Accelerator Laboratory

FERMILAB-Conf-94/159-E

CDF

Inclusive Jet and Two-Jet Differential Cross Sections at CDF

The CDF Collaboration

Fermi National Accelerator Laboratory
P.O. Box 500, Batavia, Illinois 60510

June 1994

Submitted to the *27th International Conference on High Energy Physics*, Glasgow, Scotland, July 20-27, 1994

Disclaimer

FERMILAB-CONF-94/159-E
ICHEP Ref. gls0368
Submitted to Pa-11
. Pl-13
CDF/PUB/JET/PUBLIC/2622
May 31, 1994

Inclusive Jet and Two-Jet Differential Cross Sections at CDF

The CDF Collaboration[1]

ABSTRACT

The CDF collaboration collected 19.5 pb^{-1} of data during the 1992-93 collider run at Fermilab. Using these data the inclusive jet cross section is measured in the pseudorapidity (η) range 0.1–0.7. The transverse energy (E_T) range of the jets extends from 15 to 440 GeV. The measured cross section is compared with next-to-leading order ($\mathcal{O}(\alpha_s^3)$) QCD predictions for various parton distributions and different choices of renormalization scale. A new limit on Λ_c, a term representing quark substructure, is derived. The two-jet differential cross section is measured by determining the E_T spectrum of central jets ($0.1 < |\eta| < 0.7$) for different η intervals of the second jet which span the range $0.1 < |\eta| < 3.0$. The results are compared with leading order QCD calculations.

[1]Contributed by A. BHATTI, The Rockefeller U., (BHATTI@FNALD.FNAL.GOV)

Submitted 27th International Conference on High Energy Physics, University of Glasgow, Glasgow, Scotland, July 20-27, 1994.

1 Inclusive Jet Cross Section

1.1 Introduction

The measurement of the inclusive jet cross section provides a conceptually very simple but still a fundamental test of QCD. The next-to-leading order $\mathcal{O}(\alpha_s^3)$ calculations [1],[2] have small theoretical uncertainty. The predicted cross section is not very sensitive to the choice of the renormalization/factorization scales except at very low E_T ($E_T < 50$ GeV). However there is a large ($\approx 20\%$) uncertainty due to different choice of parton distributions and this measurement can provide a useful tool to probe them. Deviations from the standard model due to quark or gluon substructure are likely to be observed in large angle parton scattering, making studies of high E_T jets an attractive method to search for hints of new physics.

The recent deep inelastic scattering (DIS) experiments (BCDMS, NMC, CCFR) have made very precise measurements of the structure functions F_2 and F_3. As a result, the parton distributions, especially the quark distributions, are known to a few percent accuracy at $x_{BJ} > 0.01$. The gluons contribute to DIS cross section through scaling violations, which are a second order effect. The gluon distributions measured in the DIS experiments are not very precise, and direct measurement of gluon distributions through direct photon production [3] is limited in x_{BJ} range to less than 0.2. The results from HERA at low x_{BJ} and high Q^2 show large values of F_2, favoring the singular gluon distributions. The parton density distributions for various partons contributing to jet production at $\sqrt{s} = 1800$ are shown in Figure 1(a) as a function of the jet E_T assuming the pseudorapidities of the jets to be $\eta_1 = \eta_2 = 0$. The contributions to the dijet cross section from various subprocesses are shown in Figure 1(b). We see that at high E_T, a region where any signature of substructure may appear, the cross section is dominated by quark-quark scattering while at low E_T, the main contribution comes from gluon-gluon scattering. Assuming that the production at low E_T can be described by QCD predictions, the jet cross section can be used to constrain the gluon distributions.

The inclusive jet cross section is defined to be

$$\frac{1}{\Delta\eta}\int d\eta \frac{d\sigma}{dE_T d\eta} = \frac{1}{\Delta\eta}\frac{1}{\mathcal{L}}\frac{N_{jet}}{\Delta E_T}$$

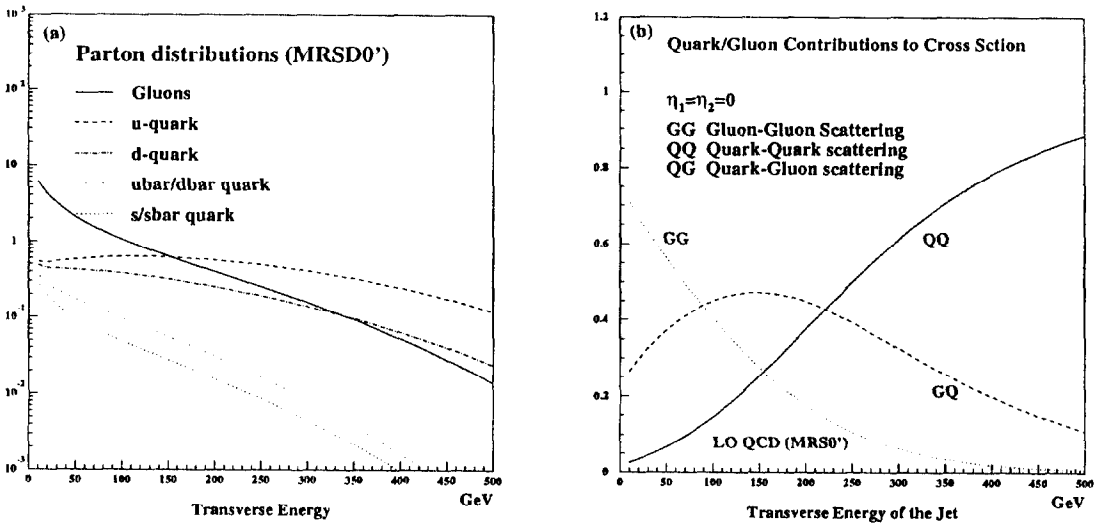

Figure 1: Contribution of various types of partons to the jet cross section as a function of E_T assuming $\eta_1 = \eta_2 = 0$

where N_{jet} is the number of jets in the E_T range ΔE_T, $\mathcal{L}$ is the luminosity and $\Delta\eta$ is the η range of the data set used. In order to ensure that the energy is well measured, only those jets are used for which $|\eta_D|$ is in the range 0.1–0.7, where η_D is the pseudorapidity of the jet calculated under the assumption that the interaction took place at $z = 0$. The CDF central calorimeter covers $|\eta_D| < 1.1$.

We have used a cone algorithm to reconstruct the jet[4] which is similar to the one used by next-to-leading order QCD calculations[1]. The jet E_T is defined as the transverse component of the sum of the energy deposited by all the particles in a cone around the jet axis. In this analysis we have used a cone of radius R=0.7. The underlying energy (energy deposited by particles generated from fragmentation of the partons not associated with hard scattering), measured in the minimum bias events, is subtracted.

1.2 Data Set and Analysis

The CDF collaboration collected 19.5 pb^{-1} of data during the 1992-1993 collider run. Four different QCD triggers, based on various jet E_T thresholds, were used. The nominal E_T thresholds were 100 (Jet_100), 70 (Jet_70), 50 (Jet_50) and 20 (Jet_20) GeV with prescale factors of 1, 6, 20 and 500, respectively. This enabled us to have adequate statistics over a large E_T range, while still having a manageable overall event rate. In the offline analysis only the data in the 25-75, 75-95, 95-120 and 120-440 GeV ranges are used from the Jet_20, Jet_50, Jet_70 and Jet_100 data samples. For the E_T range 15-25 GeV, data from minimum bias events were used. The data was corrected for trigger efficiency, measured using the overlap region with the next lower threshold trigger data.

The measured jet E_T is corrected for detector effects (energy loss, nonlinearity) and E_T smearing using the procedure described in reference [5]. A very large sample of dijet events were simulated using a jet fragmentation program based on Feynman-Field fragmentation and a detector simulation. The fragmentation parameters have been adjusted to agree with the jet fragmentation functions as measured in CDF. The detector simulation has been tuned to the single pion and electron response, as measured in test beam data and from isolated tracks in the data. These simulated events were used to parameterize the response functions which relate the measured jet energy to the true jet energy. The response functions include all the detector effects, in particular the large effect of a very steeply falling spectrum.

We assume a true inclusive jet spectrum of the form

$$\frac{d\sigma(E_T^{true})}{dE_T^{true}} = Norm * 10^{F(E_T^{True})}$$

where

$$F(x) = P_1 \log(x) + P_2 \log^2(x) + P_3 \log^3(x) + P_4 \log^4(x) + P_5 \log^5(x)$$

Given a true spectrum, we generate a smeared spectrum using the response functions described above. The parameters P_1–P_5 were determined by minimizing the χ^2. The normalization is calculated by demanding that the area under the smeared curve is equal to the one under the measured curve. The χ^2/dof of the fit is 1.14 for 36 degrees of freedom.

To evaluate the systematic uncertainty, we have used the same unsmearing procedure, using response functions generated with different input parameters. The difference between the two unsmeared curves is taken as the systematic uncertainty. The various sources of systematic uncertainty include the detector response to single pions and to electrons, modeling of detector jet energy resolution, assumptions about the shape of the response functions, jet fragmentation parameterization, and the effect of including low energy jets ($E_T^{true} < 5.0GeV$) in the unsmearing procedure. The result was found to be insensitive to unsmearing with and without the low E_T data points ($E_T < 40$ GeV). The total systematic uncertainty ranges from 32% at low E_T to 25% at high E_T, and is around 13% over most of the E_T range. The statistical uncertainty is less than 2% over most of the E_T range, except at low (high) E_T where it is 5%(33%).

1.3 Comparison with QCD

The corrected spectrum is compared to the next-to-leading order QCD calculations from [1]. As shown in Fig. 2, there is very good agreement between the measured spectrum and theory over 9 orders of magnitude. However, at a finer scale, it is seen in Fig. 3 that our data is in very good agreement with NLO QCD, using MRSD0 parton distributions, for $70 < E_T < 250$, showing a small excess at low and high E_T. This is an absolute cross section comparison. The shaded region at the bottom of Fig. 3 shows the systematic uncertainty as a function of E_T. In Fig. 4 (a), (b) NLO predictions for different choices of renormalization scale and parton distributions are compared with the theory predictions used in Fig. 3.

1.4 Compositeness Limit

The effect of the addition of a contact term to the Leading order QCD lagrangian has been calculated in reference [6]. For comparison with the data, we used MRSB0 parton distributions and we normalized the predicted cross section to the measured one over the E_T range 95-145, where the effect of a contact term is calculated to be small. Comparing the prediction with the data above $E_T > 200$ GeV, we calculate the compositeness parameter Λ_c to be larger than 1450 GeV at the 95% confidence level. The data is compared with LO QCD prediction including contact term in Fig. 5.

2 Two-Jet Differential Cross Section

2.1 Introduction

For the $2 \rightarrow 2$ process at a given $\sqrt{s}$, the momentum fraction carried by two incoming partons is completely described by η_1, η_2 and E_T. Measuring the differential cross section for production of two high E_T jets is useful for probing parton distributions. This measurement is complementary to the measurement of the dijet CM angular distribution, which probes the vector nature of gluons and is largely independent of parton distributions.

2.2 Data set and analysis

The data set used for the two-jet differential cross section is the same as the one used for the inclusive jet measurement as described above. Only a subset ($\approx 40\%$) of the 1992-93 data has been used for this study so far. The process $\bar{p}p \rightarrow$ Jet1+Jet2 + X may be described by the differential cross section $d^3\sigma/dE_T d\eta_1 d\eta_2$ where η_1 and η_2 are the pseudorapidities of the two lead jets and the E_T is the transverse energy of the leading jet. For each event we require a jet to lie in $0.1 < |\eta| < 0.7$ and have E_T above a threshold for a given trigger as described in sec. 1.2. This is called the "trigger jet". We require the second jet, called the "probe" jet, to have $E_T > 10$ GeV. The E_T distribution of the trigger jet is plotted for various slices of pseudorapidity of the probe jet. The slices of $|\eta_2|$ used are 0.1–0.7, 0.7–1.2, 1.2–1.6, 1.6–2.0 and 2.0–3.0. These slices were chosen on the basis of statistics. In the case where both jets lie in range $0.1 < |\eta| < 0.7$ and both jets satisfy the E_T threshold, this process is repeated with the second jet playing the role of trigger jet and the leading jet is used to specify the $|\eta_2|$ slice. The jets from different parts of the calorimeter are corrected to a common raw energy scale, defined by central calorimeter to minimize relative jet ordering problems in E_T. In this manner we obtain the two-jet differential cross section defined as

$$\left\langle \frac{d\sigma}{dE_T} \right\rangle = \frac{1}{\Delta\eta_2} \int d\eta_2 \frac{1}{\Delta\eta_1} \int d\eta_1 \frac{d\sigma}{dE_T d\eta_1 d\eta_2} = \frac{1}{\Delta\eta_1} \frac{1}{\Delta\eta_2} \frac{1}{\mathcal{L}} \frac{N_{jet1}}{\Delta E_T}$$

where $0.1 < |\eta_1| < 0.7$ and $|\eta_2|$ lies in different pseudorapidity slices.

Each of the five cross sections is corrected for detector effects (calorimeter energy loss and resolution) using the procedure described in section 1.2. For

this analysis, we assume that jets do not migrate between η slices because of detector η resolution. This assumption is under study. A systematic uncertainty has been estimated using the full systematic uncertainty on our published inclusive jet cross section measurement (from 1989). This uncertainty is on the cross section, and is a function of corrected E_T. The uncertainty on the cross section is converted into an effective uncertainty on the jet E_T scale by using the local slope of the inclusive jet cross section. We then apply this effective E_T uncertainty to the two-jet cross section using new local slopes. This procedure takes into account the fact that the inclusive jet spectrum has a different slope than the two-jet cross section. The size of the uncertainty at lowest E_T and the highest E_T span the following ranges for our five cross sections: $\pm 19\%$ to $+12/-18\%$; $\pm 19\%$ to $+16/-24\%$; $\pm 19\%$ to $+19/-26\%$; $\pm 21\%$ to $+32/-43\%$; and $\pm 24\%$ to $+28/-34\%$.

The systematic uncertainty on the ratio of cross sections is determined under the assumption that the errors at the same E_T value are completely correlated. However because of their different magnitudes, they do not completely cancel out. The resulting systematic error on the four ratios spans the following range from lowest E_T to highest E_T: $<1\%$ to 5%; $<1\%$ to 7%; 1-20%; and 3-37%. In the low E_T region where the slopes of the cross section are most similar, the systematic uncertainty largely cancels in the ratio.

2.3 Results and Comparison with QCD

The corrected cross section curves for various bins of $|\eta_2|$ are shown in Fig. 6. The data are compared to Leading Order QCD calculation using MT-LO parton distributions with the renormalization scale set equal to E_T. The LO QCD is a reasonable description of our data except for the highest E_T and highest $|\eta_2|$ regions. A recent $\mathcal{O}(\alpha_s^3)$ QCD calculation[7] shows that there is a substantial contribution from higher order and is in better agreement with our data.

In order to quantify the difference in shape for different pseudorapidities the ratio of various cross sections to the central η slice cross section is shown in Fig. 7. As mentioned above, the systematic errors largely cancel out and this ratio is especially immune to any error in normalization. Again the data is well described by LO QCD except for large η slice and the NLO calculation[7] (not shown) is in closer agreement.

3 Conclusions

We have measured the inclusive jet cross section in the E_T range 15-440 GeV and find it to be in good agreement with NLO QCD predictions. We set a lower limit of 1450 GeV on the compositeness parameter Λ_C.

The two-jet cross section is in good agreement with LO QCD for both the absolute cross section and the ratio of cross sections except for the highest E_T and highest η slice.

Both the systematic and the statistical uncertainties in the inclusive jet and the two-jet cross section measurements at the collider have become small enough that these measurements can now be used in a global analysis, along with DIS measurements, to determine the parton distributions.

We hope to collect 75 pb^{-1} of data during the 1994-95 run, which will enhance our chance to observe a possible composite structure of quarks.

References

[1] S. Ellis. Z. Kunszt, and D. Soper, Phys. Rev. Lett. **62** 2188 (1989), Phys. Rev. Lett. **64** 2121 (1990) .

[2] F. Aversa, P. Chiappetta, M. Greco, P. Guillet, Phys. Lett. B **210**, 225 (1988),**211**, 465 (1988); Nucl. Phys. **B327**, 105 (1989)

[3] UA6 Collaboration, G. Ballacchi *et. el.*, Phys. Lett. **B317** 250-256 (1993)

[4] CDF Collaboration, F. Abe *et. el.*, Phys. Rev. D **45** 1448 (1992).

[5] CDF Collaboration, F. Abe *et. el.*, Phys. Rev. Lett. **70** 1376 (1992) .

[6] E. Eichten, K. Lane, and M. Peskin, Phys. Rev. Lett. **50**, 811 (1983).

[7] W.T. Giele *et al.* The Two-Jet Differential Cross Section at $\mathcal{O}(\alpha_s^3)$ in Hadron Collisions; FERMILAB-PUB-94/070-T (1994)

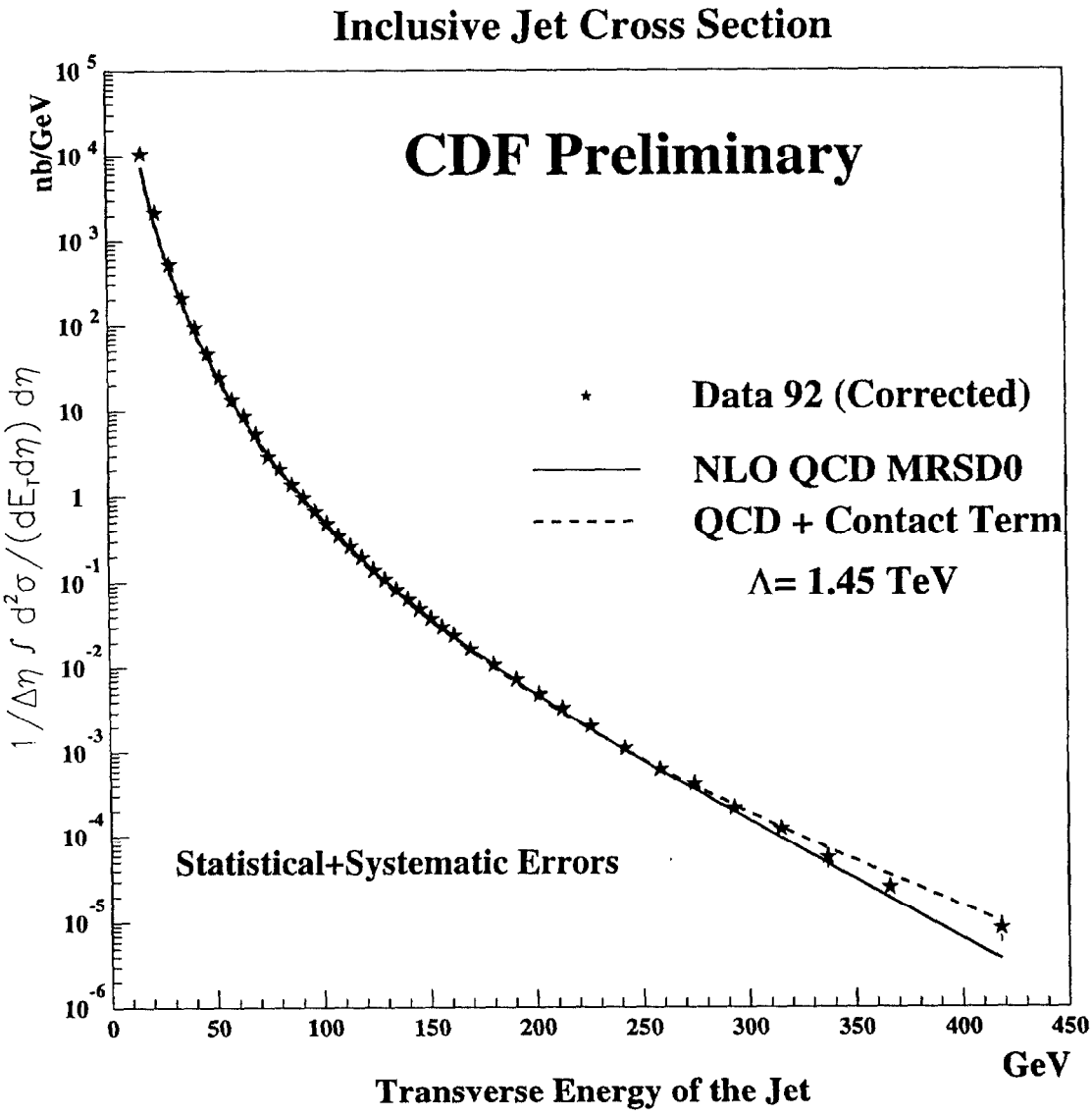

Figure 2: Comparison of Jet Cross Section with NLO QCD and with QCD+contact term predictions.

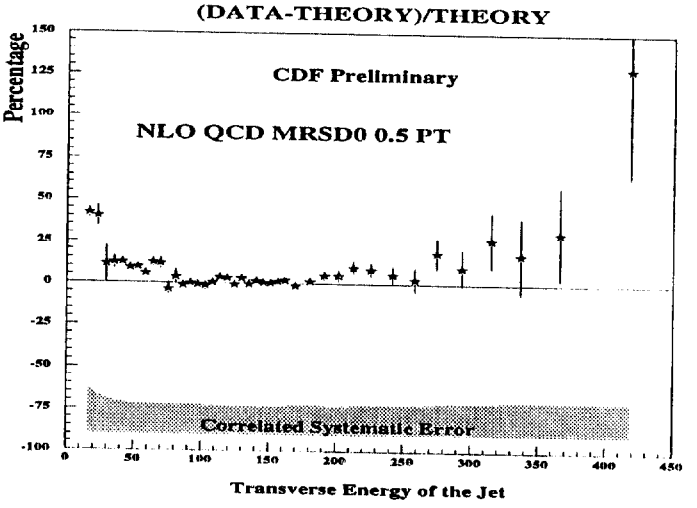

Figure 3: Comparison of Jet Cross Section with NLO QCD.

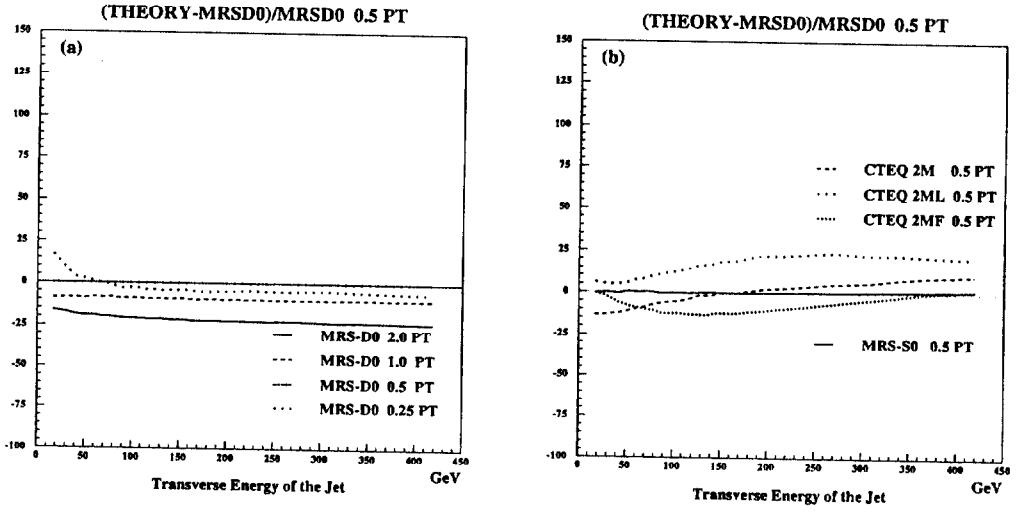

Figure 4: NLO QCD Inclusive Jet Cross Section predictions for various parton distributions.

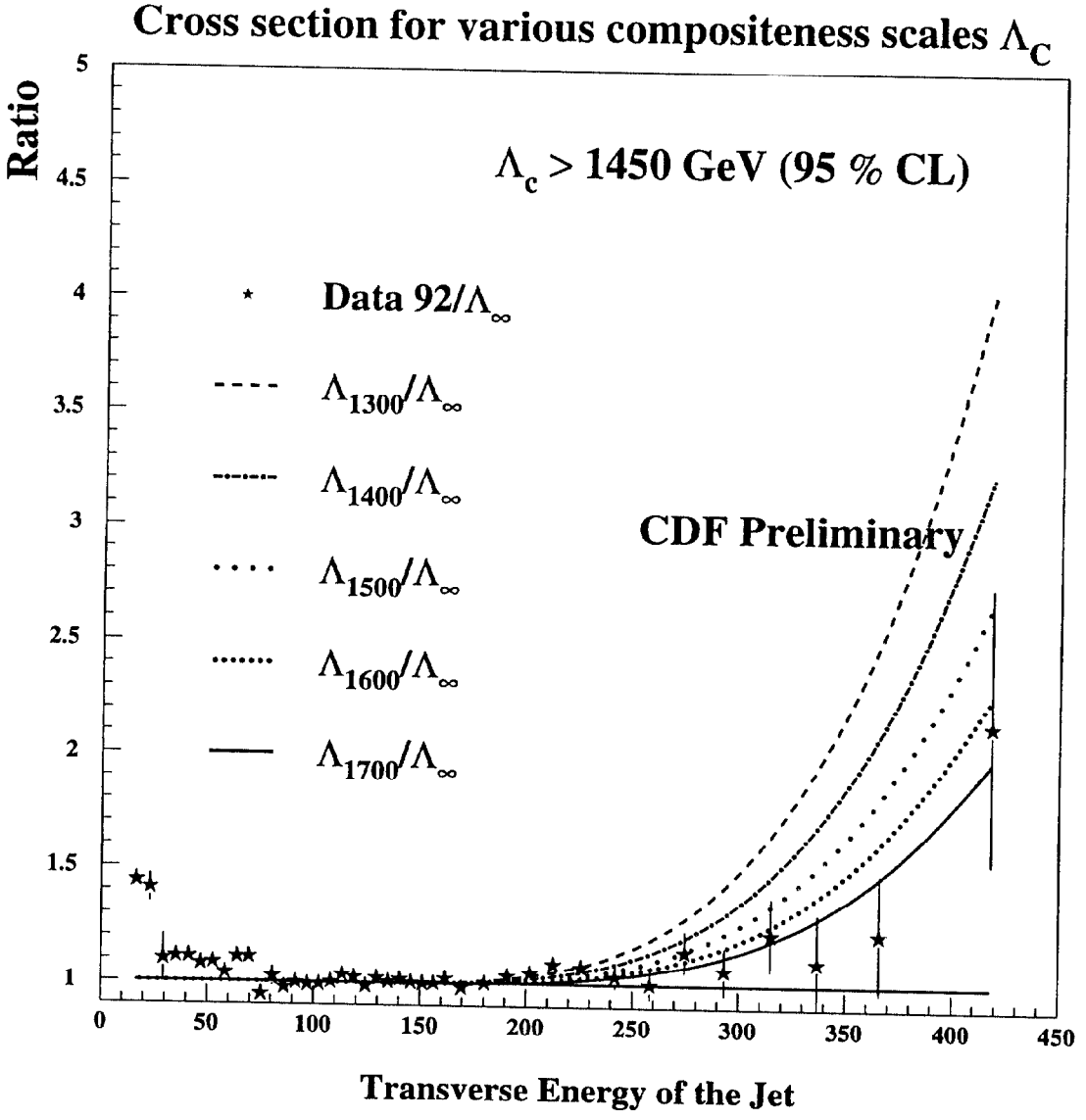

Figure 5: Comparison of Jet Cross Section with QCD+contact term predictions for various values of Λ_c.

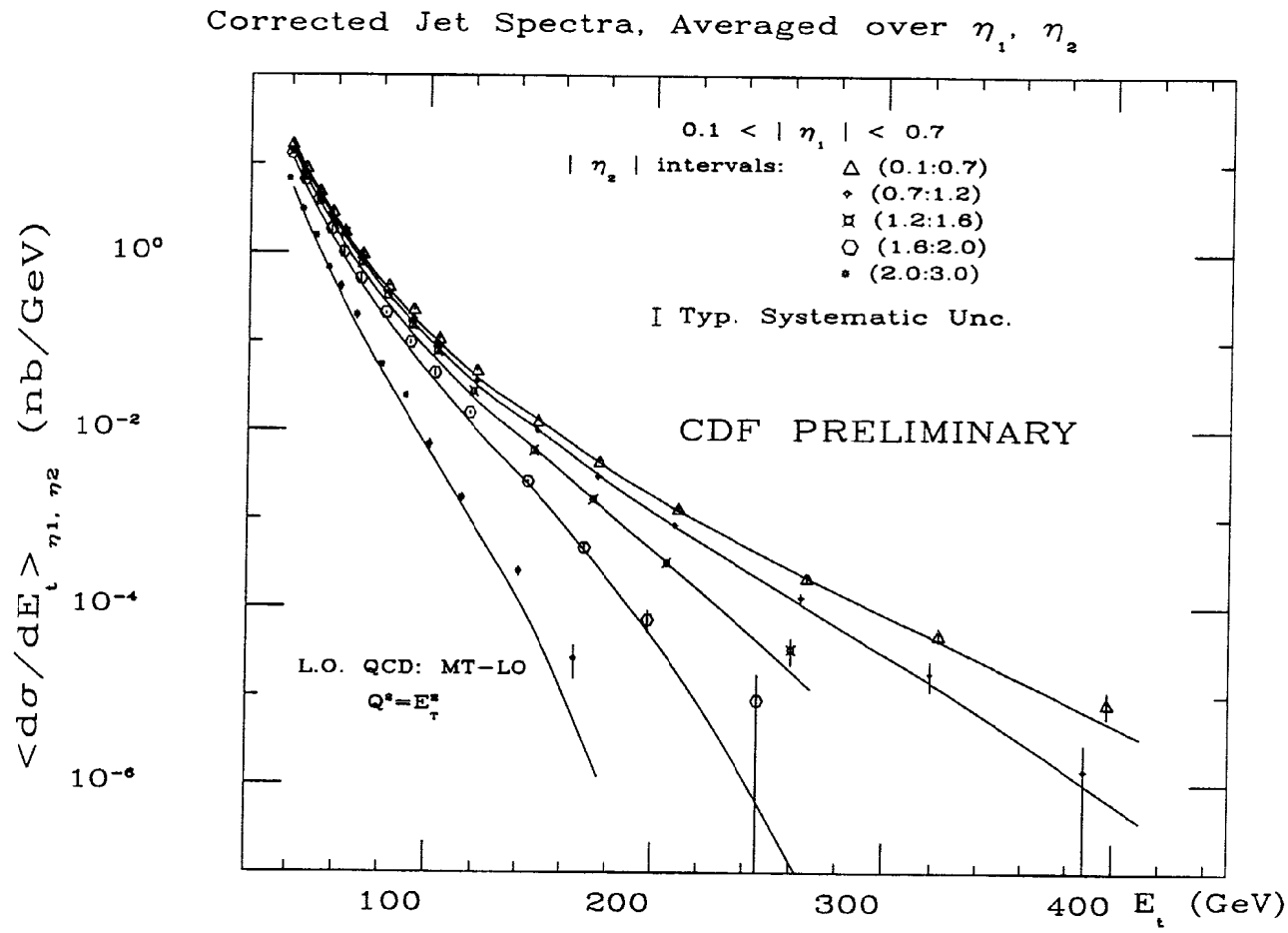

Fig. 6: Two-Jet cross section for different η slices

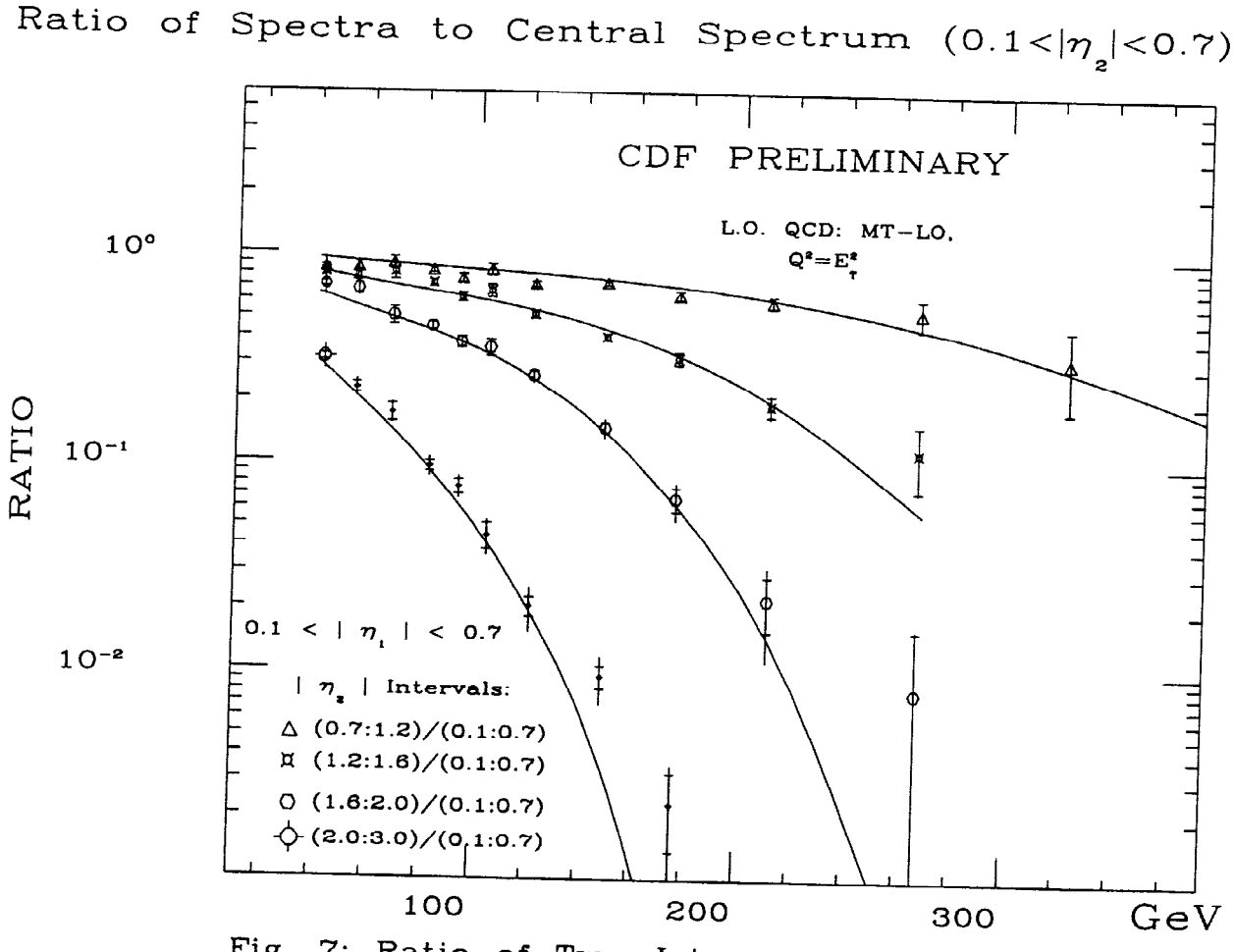

Fig. 7: Ratio of Two−Jet cross sections